

Spin dynamics in semiconductor nanocrystals

J. A. Gupta and D. D. Awschalom*

Department of Physics, University of California, Santa Barbara, California 93106

Al. L. Efros

*Naval Research Laboratory, Nanostructure Optics Section, Washington, D.C. 20375*A. V. Rodina[†]*Solid State Physics Institute, Technical University of Berlin, D-10623 Berlin, Germany*

(Received 9 April 2002; published 11 September 2002)

Time-resolved Faraday rotation is used to study both transverse and longitudinal spin relaxation in chemically synthesized CdSe nanocrystals (NC's) 22–80 Å in diameter. The precession of optically injected spins in a transverse magnetic field occurs at distinct frequencies whose assignment to electron and exciton spins is developed through systematic studies of the size-dependence and theoretical calculations. It is shown that the transverse spin lifetime is limited by inhomogeneous dephasing to a degree that cannot be accounted for by the NC size distribution alone. Longitudinal spin relaxation in these NC's occurs on several distinct time scales ranging from 100 ps to 10 μs and exhibits markedly different dependencies on temperature and field in comparison to transverse spin relaxation.

DOI: 10.1103/PhysRevB.66.125307

PACS number(s): 71.35.Ji, 42.50.Md, 78.47.+p, 78.66.Hf

I. INTRODUCTION

The size-tunable energy-level spectrum of semiconductor quantum dots (QD's) has generated interest in applications such as QD-based lasers¹ and fluorescent labels for biological molecules.² Continuing interest in the dynamics of carrier spins localized within QD's is motivated by the emerging fields of semiconductor spintronics³ and quantum computation.⁴ Proposals for the latter hope to exploit expected increases in spin-relaxation lifetimes due to fully three-dimensional confinement of electron spins. Certain channels of homogeneous spin-spin interactions may be absent in strongly confining QD's, as the discrete energy spectrum and the exclusion principle suppress the excitation of multiple electron-hole pairs within single QD's by circularly polarized, resonant photons. Recent studies have suggested that hyperfine interactions between electrons and nuclei may be the operative mechanism for carrier spin relaxation.⁵

Here we present a series of measurements that characterize both transverse and longitudinal spin dynamics in chemically synthesized nanocrystal quantum dots. It was shown in an earlier paper that spin precession following optical excitation with circularly polarized light in a transverse magnetic field occurs at up to four distinct frequencies,⁶ although assignment of the precession signatures to electrons, holes, or excitons was uncertain. Extension of the Faraday rotation technique to include independently tunable pump and probe pulses has aided the clear observation of spin precession in the full range of samples studied. Calculations of the electron g factor taking into account a size-dependent energy shift of allowable levels closely agree with the experimental data for one of the observed frequency components. Assignment of the other frequency component(s) to excitons remains uncertain; while the values obtained from the Faraday rotation are consistent with the exciton g factor obtained from magneto-absorption data, unambiguous interpretation is hindered by

considerations of anisotropy present in these nanocrystals (NC's). Efforts to calculate the exciton g factor for a randomly oriented ensemble of wurtzite NC's have led us to posit that exciton precession might only be exhibited in a special subset of "quasispherical" NC's, where anisotropy contributions from the crystal structure and physical shape cancel out.

Inhomogeneous dephasing limits the transverse lifetimes of both electron and exciton spins in these samples. By using measurements of the size-dependent electron g factor to estimate the dephasing rate, we find that dephasing from the size distribution cannot account for the observed rate in all but the smallest NC's. This suggests that contributions to electron dephasing from surface conditions⁷ and/or NC anisotropy may also be important. Longitudinal spin relaxation in NC's was studied by applying a magnetic field along the observation direction (the Faraday geometry). The decay of spin polarization in this case is found to occur on ~ 100 ps, 10 ns, and 10 μs time scales. The microsecond decay time sensitively depends on the applied field and temperature in comparison to the shorter decay components, which exhibit more gradual trends. In addition to the monotonic decay of longitudinal polarization, spin precession is found to occur in the Faraday geometry, raising questions concerning the nature of optically excited states in these NC's.

The remainder of this paper is organized into four sections. In Sec. II we describe the set of samples that have been studied and the energy spectrum of allowed states. We also review the experimental methods of time-resolved Faraday rotation and absorption that are used to monitor carrier spin and population dynamics. Section III focuses on our efforts to assign the multiple precession signatures to electrons and excitons, while Sec. IV details our measurements of inhomogeneous dephasing. Studies of longitudinal spin relaxation are presented in Sec. V, and we conclude in Sec. VI. Further

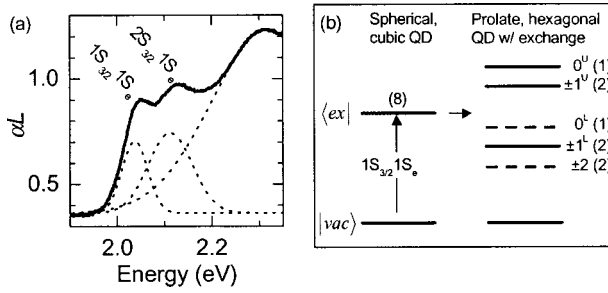


FIG. 1. (a) Absorption spectrum of 57 Å NC's at $T=6$ K. Ground and excited energies can be extracted from the respective components in a multi-Gaussian fit (dotted lines). (b) Unresolved fine-structure states within the NC exciton ground state (degeneracies are indicated in parentheses).

details of the quasispherical model for exciton spin precession are provided in the Appendix.

II. SAMPLE INTRODUCTION AND EXPERIMENTAL METHODS

Chemically synthesized CdSe nanocrystals result from the pyrolytic reaction of organometallic precursors in a coordinating organic solvent.⁸ Single crystals with the wurtzite structure were studied ranging from 22–80 Å in diameter, with a size distribution of ~ 5 –15%. The NC's are slightly prolate (elongated along the c axis),^{8a} with a size-dependent mean aspect ratio $(1+\mu)$ that may range from 1.0 to 1.3 with increasing size.^{8b} The 80 Å NC's are somewhat more prolate, with an aspect ratio of ~ 2 . Although the distribution of aspect ratios is not well characterized, a variation of ± 0.2 may be expected for samples 22–57 Å in diameter.⁹ Surface-modified CdSe/CdS core/shell NC's were also studied; the epitaxial growth of a higher band-gap shell is known to reduce the efficiency of carrier trapping by surface states, providing improved luminescence quantum yields up to 90%.¹⁰ Samples for the optical measurements were prepared by dissolving the NC's in an organic polymer which freezes into an optically transparent glass at cryogenic temperatures.

In analogy to atomic hydrogen, the discrete spectrum of states in NC's results from an approximately spherical confinement potential provided by the band-gap contrast between the semiconductor and insulating matrix. The net wave function of excitons occupying these states is described by the product of electron and hole wave functions comprised of parts related to the intrinsic unit cell of the solid and an envelope function that satisfies boundary conditions imposed by the nanocrystals' finite size. As an example, the ground exciton state is denoted as $1S_{3/2}1S_e$, where the term $1S$ refers to the hydrogenic shell state and the subscripts refer to either $J=\frac{3}{2}$ holes or $S=\frac{1}{2}$ electrons.^{11,12} Ground and excited states are visible in the linear absorption spectrum of samples with relatively good size distributions as inhomogeneously broadened peaks [Fig. 1(a)]. In perfectly spherical NC's with cubic crystal structure and negligible electron-hole exchange, the $1S_{3/2}1S_e$ ground exciton state is eightfold degenerate, comprising the possible combinations of hole and electron spins. This degeneracy can be broken in CdSe

NC's resulting in a multiplet of five fine-structure states whose relative order and spacing depends on the wurtzite crystal structure, prolate shape, and e - h exchange interaction [Fig. 1(b)]. Although these states cannot be directly resolved in absorption spectra, they have been observed using size-selective techniques to circumvent broadening due to the size distribution.¹³ The states are labeled by their angular momentum projection onto the crystal c axis (0 , ± 1 , or ± 2); the superscripts U or L refer to higher- and lower-energy states with the same projection.^{13,14} In NC's whose c axis is oriented along the observation direction, optical selection rules are well defined and dictate that circularly polarized σ^\pm light will couple to the ± 1 states, respectively. Selection rules are poorly defined in the large majority of NC's whose c axis is oriented at a random angle; superpositions of both states may be excited in such NC's. Previous work suggests that radiative recombination of optically excited carriers occurs upon relaxation to the ± 2 “dark exciton” states;¹⁵ the time scale for such relaxation is not well known but may be of order ~ 200 ps.¹⁶

Pump-probe techniques were employed to monitor carrier population and spin dynamics in the time domain. Synchronized optical parametric amplifiers with a repetition rate of 250 kHz produce ~ 150 fs pump and probe pulses with energies E_{pump} and E_{probe} that are independently tunable across the visible spectrum. A pulsed white light continuum is also produced that can alternatively serve as a probe pulse. The pump and probe pulses are normally incident on the sample and focused to a ~ 100 μm spot using an achromatic doublet lens. Conventional mechanical delay lines control the relative time delay t between pump and probe pulses and optical choppers are used to modulate both pulse trains, enabling the use of lock-in amplifiers. The sample sits in the bore of a magneto-optical cryostat capable of magnetic fields up to $H=7$ T and temperatures $T=2$ –300 K.

Carrier population dynamics were monitored through time-resolved absorption (TRA) as a pump-induced change in the absorption spectrum detected at an energy E :

$$\Delta\alpha(E,t)L \equiv (\alpha_0 - \alpha(t))L = \ln\left(\frac{T(t) - T_0}{T_0} + 1\right). \quad (1)$$

Here L is the sample thickness and α (α_0) is the semiconductor absorption spectrum in the presence (absence) of the pump. In practice, $\Delta\alpha L$ is computed from the corresponding transmitted probe intensities $T(t)$ and T_0 ; positive values typically represent state-filling effects where the probe is preferentially transmitted due to the occupation of states by pump-excited carriers that would otherwise be available for absorption of probe photons. The white light continuum serves as the probe in these experiments, facilitating measurement of $\Delta\alpha L$ across the entire NC absorption spectrum. Changes in the transmitted probe intensity are detected using either a photomultiplier tube or photodiode array which are attached to a 0.5-m spectrometer.¹⁷ Both pump and probe pulses are circularly polarized, with a relative helicity that can be controlled using variable retarders.

Carrier spin dynamics are monitored with the technique of time-resolved Faraday rotation (TRFR).¹⁸ The circularly po-

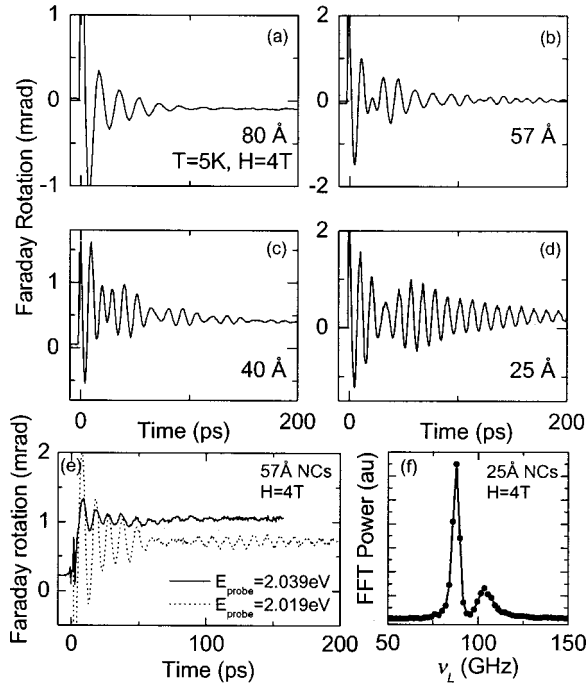


FIG. 2. (a)–(e) Time-resolved Faraday rotation in the Voigt geometry. $T=5$ K, $H=4$ T. Laser parameters are 80 Å, $E_{\text{pump}}=E_{\text{probe}}=2.00$ eV; 57 Å, $E_{\text{pump}}=2.07$ eV, $E_{\text{probe}}=2.10$ eV; 40 Å, $E_{\text{pump}}=E_{\text{probe}}=2.14$ eV; 25 Å, $E_{\text{pump}}=E_{\text{probe}}=2.48$ eV. (e) $E_{\text{pump}}=2.175$ eV, $E_{\text{probe}}=2.019$ or 2.039 eV, $P_{\text{pump}}=0.5$ mW, $P_{\text{probe}}=20$ μ W. (f) FFT power spectrum of data in (d) showing two distinct precession frequencies.

larized pump pulse typically excites a population of electron-hole pairs that are spin polarized along the optical path. The resultant spin magnetization and spin-selective state-filling effects produce a circular birefringence in the sample whose component along the optical path is detected as the rotation of a linearly polarized probe pulse. Sensitivity to rotation angles >10 μ rad is achieved using a balanced photodiode bridge. If the magnetic field is applied along the observation direction (Faraday geometry), the pump-excited spins comprise a highly nonequilibrium population whose relaxation involves energy transfer to the lattice via phonons. In the simplest case, such relaxation follows an exponential decay with a time constant T_1 . When the magnetic field is applied perpendicular to the observation direction (Voigt geometry), the pump-excited spins comprise a coherent superposition of states whose temporal evolution corresponds to Larmor spin precession at a frequency $\nu_L = g\mu_B H/h$ proportional to the spin g factor (μ_B is the Bohr magneton). Transverse spin relaxation yields a lifetime T_2^* which may contain contributions from longitudinal and purely transverse spin relaxation, as well as inhomogeneous dephasing.

III. MULTIPLE PRECESSION FREQUENCIES

Figures 2(a)–2(d) show characteristic spin precession in the Voigt geometry for CdSe NC's 25 – 80 Å in diameter. It has previously been shown that low-field spin lifetimes in these samples are ~ 3 ns;⁶ the ~ 50 ps lifetimes here are a

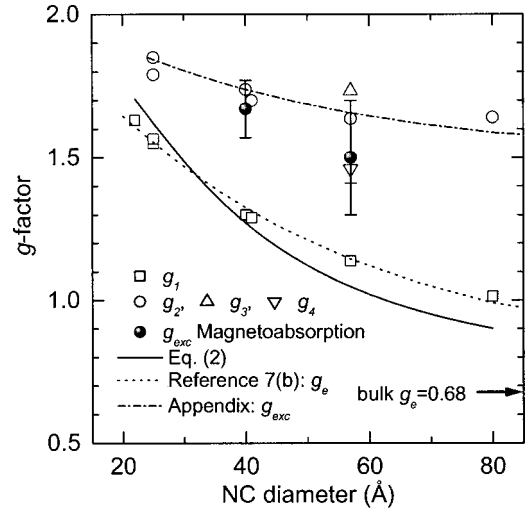


FIG. 3. Compilation of g factors measured in CdSe NC's. The open symbols are from analysis of spin precession frequencies, while the two closed symbols are extracted from spin splittings in magnetoabsorption spectra. The solid and dotted lines are calculations of the size-dependent electron g factor using Eq. (2) and Ref. 7b, respectively. The dashed line is a calculation of an exciton g factor using Eq. (3) with $g_h = -0.73$.

result of inhomogeneous dephasing, discussed in Sec. IV. Data are usually taken with the pump and probe energies in the vicinity of the $1S_{3/2}1S_e$ exciton state. The visibility of the spin precession oscillations can depend sensitively on the choice of detection energy. This is illustrated in Fig. 2(e) for two choices of E_{probe} near the ground state in 57 Å NC's (2.05 eV). Because the Faraday rotation signal is proportional to the difference in refractive indices for the right- and left-circularly polarized components of the linearly polarized probe,¹⁹ the magnitude and sign can change with E_{probe} in the vicinity of an absorption resonance. The ability to independently tune pump and probe energies has proven useful in maximizing the prominence of spin precession, particularly in the smaller NC's <40 Å in diameter, where initial experiments reported only marginal results.⁶ It is often the case that there is a monotonically decaying background contribution to the Faraday rotation signal in this geometry. A possible origin of this signal will be discussed in the context of the Faraday geometry measurements in Sec. V.

Modulation of the oscillation envelope indicates the presence of multiple frequency components that are directly resolved in a fast Fourier transform (FFT) of the data [Fig. 2(f)].²⁰ FFT's of spin precession over a broad range in detection energy reveal no variation in spectral content; only the amplitude of the oscillatory signal is affected. Precise measurement of the g factors associated with these components can be obtained by plotting the positions of peaks in the FFT spectrum versus magnetic field. Figure 3 and Table I show a compilation of g factors measured in our sample set. Two g factors have been observed in NC's ranging from 25 – 80 Å, with the notable exception of the 57 Å NC sample, where four g factors were visible.

We assign the lower-frequency precession to the electron g factor, which is considerably shifted from the bulk value of

TABLE I. Compilation of g factors observed in CdSe NC's from spin precession measurements taken at $T=5$ K.

	22 Å	25 Å	25 Å Core/shell	40 Å	40 Å Core/shell	57 Å	80 Å
g_e	1.63 ± 0.01	1.565 ± 0.002	1.631 ± 0.004	1.30 ± 0.01	1.458 ± 0.004	1.138 ± 0.006	1.014 ± 0.006
g_2		1.83 ± 0.01	1.85 ± 0.01	1.72 ± 0.01	1.78 ± 0.01	1.636 ± 0.007	1.64 ± 0.02
g_3						$1.734 \pm .004$	
g_4						1.46 ± 0.05	

$g_e = 0.68$ in CdSe.²¹ This shift and the trend with size can be qualitatively understood by modifying equations for g_e in bulk semiconductors²² to account for the confinement-induced shift of electron energy within the conduction band.²³

$$g_e = g_0 - \frac{2}{3} \frac{E_p \Delta_{so}}{(E_g + E + \Delta_{so})(E_g + E)}. \quad (2)$$

Here $g_0 \sim 2$ is the free-electron g factor, E is the electron energy measured from the bottom of the bulk conduction band, E_g is the semiconductor band gap, E_p is the Kane energy parameter, and Δ_{so} is the spin-orbit splitting of the valence band. The electron g factor implicitly depends on the NC radius R through the size-dependent electron energy, which can be written as $E \sim a/R^2$ in the simplest parabolic approximation.¹⁴ The solid curve in Fig. 3 shows a calculation of g_e from Eq. (2) which treats $a = 267 \text{ eV \AA}^2$ as the only fitting parameter and uses literature values of $E_g = 1.839 \text{ eV}$ (for bulk CdSe at 10 K),¹² $\Delta_{so} = 0.42 \text{ eV}$,¹² and $E_p = 19.1 \text{ eV}$.²⁴ The dotted line was calculated using a better description of the size-dependent electron energy and consideration of finite boundary conditions at the NC surface.^{7b} It has been shown that the latter may result in changes to calculated values of g_e by $\sim 5\text{--}10\%$ in NC's;⁷ a variable characterizing this contribution was treated as the only fitting parameter in the calculations. Our assignment of this precession component to electron spins is based on the good agreement between the experimental data and these calculations. Higher values of g_e found in the CdSe/CdS core/shell NC's (Table I) are most likely due to electron penetration into the CdS shell, as (bulk) CdS has a larger g_e value of 1.76.²⁵

As a first step toward the assignment of the second precession component to exciton spins, we have performed magnetoabsorption experiments in the Faraday geometry that should be simply connected with the band-edge exciton spin splitting.²⁶ Gaussian peaks are fit to inhomogeneously broadened absorption spectra [cf. Fig. 1(a)] taken with σ^+ and σ^- light helicities. The splitting between spin-up and spin-down exciton states was extracted from the center positions of the ground-state exciton peak and plotted versus field.²⁷ Large fields ($H > 3 \text{ T}$) were needed in order to observe the spin splitting ($< 1 \text{ meV}$), which is much smaller than the inhomogeneous absorption linewidth ($\sim 50 \text{ meV}$). Included in Fig. 3 are values of g_{exc} calculated from magnetoabsorption data for 40 Å and 57 Å NC's. Within experimental error, the

values of g_{exc} obtained from this procedure are consistent with the larger g -factor components measured from Faraday rotation data.

Assignment of the g factors $g_2\text{--}g_4$ to exciton precession is complicated by two factors: (i) random orientation of NC's in the plastic films, (ii) the multiplet of possible states within the ground-state exciton.¹⁴ The random orientation is a problem because the exciton g factor is expected to be strongly anisotropic in CdSe NC's due to the nonspherical shape and wurtzite crystal structure.²⁵ Thus, measured values of the exciton g factor for individual NC's can depend on the orientation of the c axis relative to the applied field and observation directions. For our ensemble measurements, this anisotropy must be averaged over a random distribution. Furthermore, the shape, crystal structure, and exchange interaction in NC's result in a multiplet of fine-structure states whose relative spacing *and ordering* can depend on the exact size and shape of the NC [Figs. 4(a) and 4(b)]. We expect that the variation in the aspect ratio present within our samples is large enough that different NC's within the ensemble can have a significantly different arrangement of these fine-structure levels. Depending on how quickly (or if) relaxation occurs from optically excited states to the lowest-energy state, different exciton g factors may be obtained because each of these levels will exhibit a characteristic spin splitting with magnetic field. Association of the larger g -factor component with exciton states provides the possibility for explaining the multiple g factors $g_2\text{--}g_4$ observed in the 57 Å NC's (cf. Table I) in terms of the fine-structure levels, although it is unclear why this is the only size in which g_3 and g_4 could be resolved.

It should be noted that electron and exciton precession must not occur together within the same NC. It is possible that exciton precession is only exhibited in a special subset

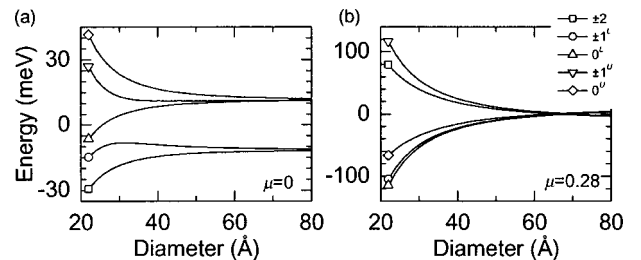


FIG. 4. Calculations of exciton fine-structure states versus size, adapted from Ref. 14. (a) Spherically shaped NC's ($\mu=0$). (b) Prolate NC's ($\mu=0.28$).

of NC's, while electron precession is expressed by the majority of NC's in the ensemble. Because our efforts to average an anisotropic exciton g factor did not qualitatively agree with the experimental data,²⁸ we speculate that exciton spin precession may only occur within quasispherical NC's where the anisotropy due to the physical shape exactly cancels that due to the wurtzite crystal structure. Such cancellation is possible because the two terms have opposite signs in CdSe NC's.¹⁴ For a given NC diameter, a choice of aspect ratio within the range expected for the ensemble can be found where the anisotropy due to shape and crystal structure offset. The exciton g factor in this subset of NC's may be perfectly isotropic, thus simplifying the interpretation by obviating the averaging of energy-level structure and anisotropy over the ensemble that would otherwise be necessary. The dotted line in Fig. 3 shows a calculation of the ground-state exciton g factor from the spin splitting of $\pm 1^L$ fine-structure levels in quasispherical NC's using the relation

$$g_{\text{exc}} = (g_e - 3g_h)/2. \quad (3)$$

The hole g factor was treated as a size-independent fitting parameter; all size dependence was assumed to come from g_e . Details of this calculation will be discussed in the Appendix; while the agreement is promising, a definitive assignment of the higher g -factor component to exciton precession requires further study.

Exciton spin precession with a ~ 50 ps spin lifetime has previously only been observed in thin GaAs/AlGaAs quantum wells under stringent conditions of low-energy excitation and low temperature, which stem from the sensitivity of the hole spin to energy relaxation and thermal processes.²⁹ If our assignment of higher-frequency precession to excitons is correct, the dependencies of exciton spin lifetimes on temperature and excitation energy are completely different in NC's. It was shown earlier that both electron and exciton precession persist to room temperature with nanosecond-scale lifetimes at low field.⁶ Here we will also show that spin relaxation in these NC's is surprisingly indifferent to energy relaxation, even when initial excitation occurs hundreds of meV above the ground-state exciton energy.

To monitor possible changes in carrier population dynamics with excitation energy, Fig. 5 shows TRA data taken at three different pump energies, indicated by the arrows in Fig. 5(a). Positive peaks in Figs. 5(b)–5(d) occur due to state-filling effects and correspond to the position of the $1S_{3/2}1S_e$ and $2S_{3/2}1S_e$ states estimated from the absorption spectrum [cf. Fig. 1(a)]. Even though the carrier population resides in the ground state, absorption of probe photons at the $2S_{3/2}1S_e$ states' energy is suppressed due to the shared $1S_e$ level.³⁰ Because the choice of excitation energy in Fig. 5(b) selectively excites larger NC's in the size distribution, the state-filling peaks are redshifted relative to Figs. 5(c) and 5(d). The difference in $\Delta\alpha L$ with probe polarization evidenced by data taken at $t = 20$ ps indicates that the population of spin-polarized carriers is a small fraction of the total carrier population. In principle, the maximum spin polarization of 100% can be achieved in bulk CdSe for near-resonant excitation along the c axis; the small amount here probably reflects the

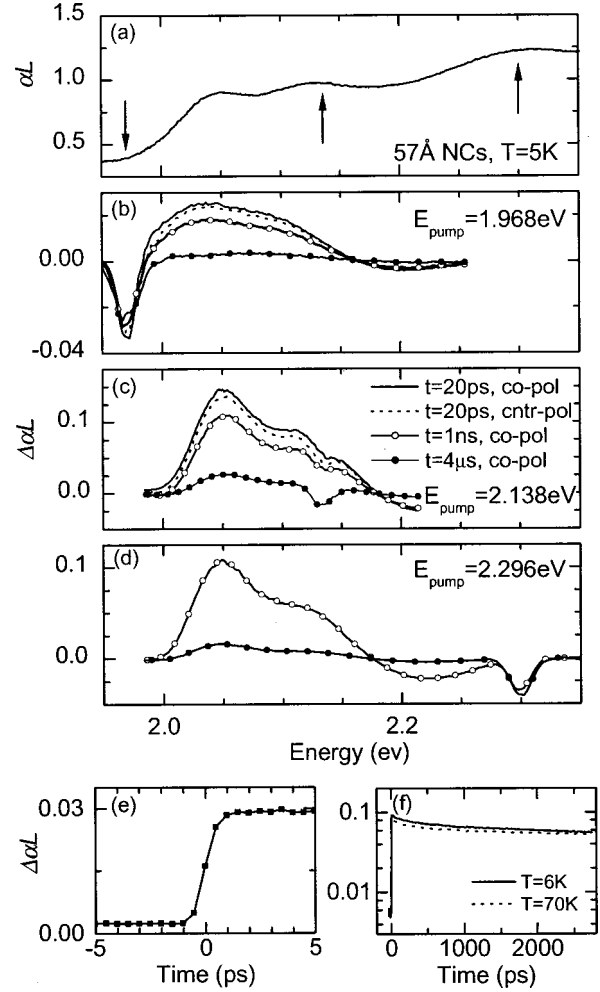


FIG. 5. (a) Absorption spectrum of 57 Å NC's with pump energies in (b)–(d) marked by arrows for reference. (b)–(d) Pump-induced changes in absorption taken at fixed time delay with either a cocircularly or countercircularly polarized probe. Use of the white light continuum here allows broad spectral coverage of $\Delta\alpha L$. $P_{\text{pump}} = 0.6$ mW. (b) $E_{\text{pump}} = 1.968$ eV. (c) $E_{\text{pump}} = 2.138$ eV. (d) $E_{\text{pump}} = 2.296$ eV. (e) Time scan showing ultrafast energy relaxation. $E_{\text{pump}} = 2.296$ eV, $E_{\text{probe}} = 2.109$ eV, $P_{\text{pump}} = 0.5$ mW, $P_{\text{probe}} = 30$ μ W. (f) Comparison of decays in $\Delta\alpha L$ at $T = 6$ and 70 K. $E_{\text{pump}} = 2.142$ eV, $E_{\text{probe}} = 2.105$ eV, $P_{\text{pump}} = 0.9$ mW, $P_{\text{probe}} = 100$ μ W.

randomly oriented ensemble of NC's in these samples. It is interesting to note that the TRA signal persists over the entire laser repetition interval of 4 μ s, indicating that carriers populate NC's on this time scale. This may be consistent with the ~ 1 μ s decay times measured from time-resolved photoluminescence experiments,^{15,31} although evidence is shown in Sec. V that spin polarization can last for even longer times. The negative feature which tracks the excitation energy is not well understood; the lack of polarization and longevity of the signal might be signatures of spectral-hole burning, although such signals are generally positive.³² As established in previous studies,³³ energy relaxation down to the $1S_{3/2}1S_e$ state occurs quickly (< 1 ps), accounting for the similar $\Delta\alpha L$ signals in Figs. 5(c) and 5(d) and directly verified in Fig. 5(e) by the fast rise time (~ 500 fs) of the state-filling signal with

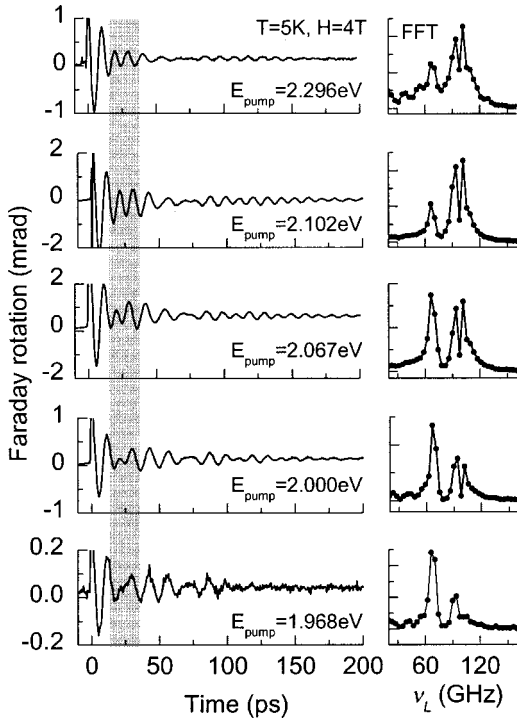


FIG. 6. Dependence of TRFR on E_{pump} in 57 Å NC's. $P_{\text{pump}} = 0.5$ mW, $P_{\text{probe}} = 30$ μ W, $E_{\text{probe}} = 2.109$ eV, $H = 4$ T, $T = 6$ K. The gray bar highlights the changing beat pattern between exciton and electron precession. Right: Corresponding FFT power spectra show an increase in exciton precession with E_{pump} .

high E_{pump} . Figure 5(f) shows that the initial decay of $\Delta\alpha L$ due to carrier recombination is independent of temperature up to the measured 70 K. The longer decay component is ~ 12 ns, indicating that the ~ 3 ns transverse spin lifetimes in these NC's at low field are not limited by carrier recombination.

Figure 6 shows complementary Faraday rotation data taken over the same range of excitation energy. Spin precession lifetimes are roughly constant over this range of E_{pump} , indicating that spin coherence is preserved during the rapid energy relaxation process, even when initial excitation occurs into higher exciton states within the NC (i.e., top panel). This surprising result holds despite the complex spectrum of states accessible to higher-energy pump photons. In addition to the fine-structure levels present within the ground $1S_{3/2}1S_e$ exciton state, each of the higher excited states has its own characteristic multiplet of fine-structure levels. The overlap of these levels for different NC's within the ensemble makes the detailed treatment of energy and spin relaxation in these NC's intractable. FFT's of the spin precession data indicate that while the exciton spin lifetime is largely unchanged, the relative spectral weight of exciton precession decreases with decreasing E_{pump} , a trend that has also been observed in the 80 Å and 40 Å NC's. Speculations on this effect in the context of the quasispherical model will be discussed in the Appendix. For now, we note that this trend reinforces the notion that exciton and electron spin precession may be exhibited by different NC's within the ensemble.

IV. INHOMOGENEOUS DEPHASING

Inhomogeneous dephasing occurs when an ensemble of spins precess at a continuous distribution of frequencies. Dephasing leads to an artificially short decay time, even though the individual spins may still have a well-defined phase relative to their initial direction. In conventional nuclear magnetic resonance, dephasing commonly results from inhomogeneity in the external magnetic field. Even small variations in field suffice to limit measured transverse spin lifetimes because intrinsic nuclear spin lifetimes are long and the samples are large. For the electron spin lifetimes and small sample volume measured in these optical experiments, inhomogeneity of the applied field can be neglected. The dephasing of spin precession in these NC's is caused by intrinsic sample inhomogeneity, the most straightforward example of which is the size distribution.

As demonstrated in Fig. 3, both electron and exciton g factors are dependent on the NC diameter, so that the sample size distribution will result in a corresponding distribution in g factors. To estimate how the resultant inhomogeneous dephasing affects the ensemble spin magnetization, we start by assuming a Gaussian distribution of g factors over N spins:

$$N(g) = \frac{N}{\sqrt{2\pi}\Delta_g} \exp[-(g-g_0)^2/2\Delta_g^2]. \quad (4)$$

Here Δ_g is the standard deviation of the distribution centered about g_0 . The net magnetization at each value of g is

$$M(t, g) = N(g) \exp(-t/T_2^*) \cos(g\mu_B H t / \hbar), \quad (5)$$

so that the ensemble magnetization is obtained by integrating $M(t, g)$ over all possible g :

$$M(t, g_0) = \frac{N}{\sqrt{2\pi}\Delta_g} \int_{-\infty}^{\infty} e^{-(g-g_0)^2/2\Delta_g^2} e^{-t/T_2^*} \times \cos(g\mu_B H t / \hbar) dg \quad (6)$$

$$M(t, g_0) = N e^{-t/T_2^*} \times \exp[-t^2/2(\hbar/\mu_B H \Delta_g)^2] \cos(g_0 \mu_B H t / \hbar).$$

When dephasing dominates the spin dynamics, the precession envelope acquires a Gaussian shape with a standard deviation Δ_t that is inversely proportional to the applied field:

$$\Delta_t = \frac{\hbar}{\mu_B H \Delta_g}. \quad (7)$$

In practice it is easier to measure the frequency linewidth of the Fourier transform (FT), since it is tedious to fit the complicated spin precession dynamics in the time domain. While the FT of spin precession data in the absence of dephasing follows a Lorentzian function if T_2^* is well defined, the FT under dephasing due to a Gaussian distribution of g factors is Gaussian with a standard deviation in frequency:

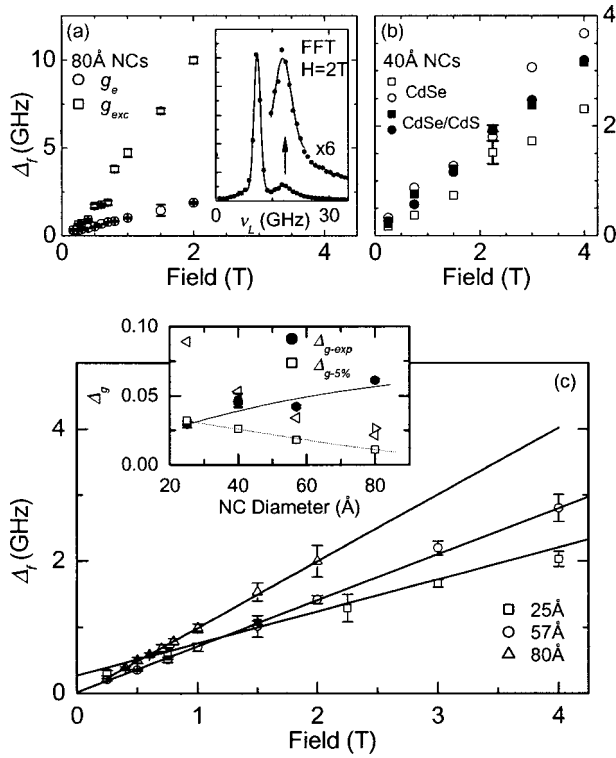


FIG. 7. Plots of FFT linewidth (Δ_f) versus field reveal inhomogeneous dephasing in CdSe NC's. (a) Electron and exciton dephasing in 80 Å NC's. Inset: Peaks in the FFT power spectrum and Gaussian fits (solid line) of central regions used to extract Δ_f . (b) Comparison of dephasing in 40 Å core and core/shell NC's. (c) Size dependence of the electron dephasing rate. Inset: Variance in g_e calculated from spin precession data (closed symbols) and expected from size distributions of 5% (open squares), 10% (left triangles), and 15% (right triangle). The lines are guides to the eye.

$$\Delta_f = (2\pi\Delta_t)^{-1} = \frac{\mu_B H \Delta_g}{h}. \quad (8)$$

The deviation Δ_g can thus be calculated from a plot of Δ_f versus H .³⁴

In order to quantify dephasing rates in these NC's, we apply this model of dephasing for both electron and exciton precession using FFT's of spin precession data, shown in the inset of Fig. 7(a). The two peaks in the FFT consistently resolvable in the sample set were fit with Gaussian functions to extract the linewidths.³⁴ Note that although the central regions of each peak are reasonably well fit, this procedure is only an approximation because the complete line shapes are neither purely Gaussian nor Lorentzian. Results are shown in Figs. 7(a) and 7(b) for electron and exciton components in 80 Å and 40 Å NC's. *A priori*, the linear relationship in these plots suggests that dephasing in these samples does result from Gaussian distributions centered about the nominal electron and exciton g factors. In nearly all of the samples studied,³⁵ the dephasing rate associated with the exciton g factor component is larger. This cannot be explained if exciton dephasing arises solely from the size distribution, since g_{exc} depends less sensitively on size than does g_e (Fig. 3). If the multiple exciton-like g factors resolved in 57 Å NC's are

present but unresolved in the other NC samples then there may be a contribution to the exciton linewidth from the field-dependent splitting of the triplet that could account for at least part of the discrepancy.

When compared to core-only NC's, the electron dephasing rate is significantly higher in core/shell NC's [Fig. 7(b)], which may be attributed to fluctuations in shell thickness and thus g_e among the ensemble. Figure 7(c) shows that electron dephasing in core-only NC's decreases with size. This also is unexpected from the size dependence of g_e if one assumes a constant size distribution in each of the samples because the slope of the curve in Fig. 2 increases with decreasing size. Although the exact size distribution in these samples is not well characterized, it is expected to fall between ~ 5 –10% for (25–57) Å NC's and ~ 15 % for 80 Å NC's.³⁶ We estimate the standard deviation in g_e from the size distribution by assuming a Gaussian deviation of 5%, which can be converted into Δ_{g-size} using the data in Fig. 3 as a calibration curve. This is compared to the values Δ_{g-exp} directly obtained from spin precession data using Eq. (8). The inset to Fig. 7(c) shows that $\Delta_{g-size} \ll \Delta_{g-exp}$ for all but the smallest NC's studied, suggesting that electron spin dephasing in these samples is not solely due to the size distribution. Incidentally, a 10% size distribution results in a dephasing rate that is too high for the smaller NC's (left triangles in the inset), however the choice of size distribution should be subject to the constraint that $\Delta_{g-size} \leq \Delta_{g-exp}$. No reasonable choice of size distribution can account for the observed dephasing rate in the 80 Å QD's, Δ_{g-size} for the expected 15% size distribution in this sample is shown as the right triangle in the inset. An additional contribution to the observed dephasing rate may come from the wurtzite crystal structure; previous calculations for bulk semiconductors suggest that the crystal-field splitting of heavy and light-hole valence bands by an energy Δ_{cr} results in a slight anisotropy of g_e relative to the c axis.³⁷ Using expressions for g_e^\parallel and g_e^\perp in Ref. 37, it can be shown that if one substitutes $E_g + E$ for E_g as was done in Eq. (2) and uses the approximation $\Delta_{so} \gg \Delta_{cr}$, which is valid for bulk CdSe ($\Delta_{so} \sim 420$ meV, $\Delta_{cr} \sim 25$ meV), this anisotropy,

$$\Delta g_e = g_e^\perp - g_e^\parallel \approx \frac{E_p \Delta_{cr}}{2(E_g + E)(E_g + E + \Delta_{cr})}, \quad (9)$$

decreases with increasing energy in the conduction band. Thus the dependence of electron energy on quantum confinement will lead to a decrease in anisotropy and its contribution to dephasing with decreasing size, in qualitative agreement with the observed trends. However, one has to also account for valence-band splitting due to the nonspherical NC shape, so that Δg_e must be averaged over an ensemble of sizes and shapes before its contribution to electron dephasing can be estimated. As a rough indication of scale, we estimate that (without averaging) Δg_e can be of order 1–5% for a typical NC. Finally, the calculations in Ref. 7 indicate that a comparable change in g_e can be obtained with modest adjustment of parameters that characterize the region at the surface over which the electron wave function goes toward zero. Further studies beyond the scope of this paper are re-

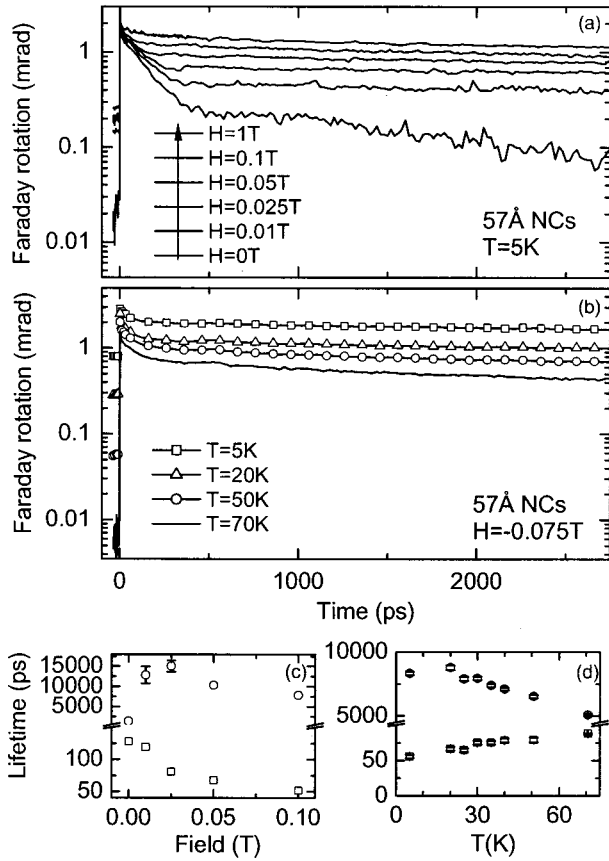


FIG. 8. TRFR in 57 Å NC's taken in the Faraday geometry with $P_{\text{pump}} = 1.0$ mW, $P_{\text{probe}} = 120$ μ W, $E_{\text{pump}} = 2.138$ eV, $E_{\text{probe}} = 2.102$ eV. (a) The decay time of longitudinal spin polarization increases with field from $H = 0$ T (bottom) to $H = 1$ T (top). (b) Temperature dependence taken at fixed field. (c), (d) Longitudinal spin lifetimes extracted from fits to (a) and (b) assuming a biexponential decay. Systematic changes with temperature and field in the signal at negative delay reveal an additional microsecond scale decay component.

quired to average the anisotropy and surface effects in order to calculate the possible contributions to dephasing in these NC's.

V. LONGITUDINAL SPIN RELAXATION

As discussed in Sec. II, measurements of spin dynamics in the Faraday geometry can be used to quantify longitudinal spin relaxation, which in the simplest cases proceeds with a decay time T_1 . Such relaxation results from the exchange of energy between a spin population and the host lattice as the system seeks to achieve a thermal equilibrium value of spin polarization. Figures 8(a) and 8(b) show the dependence of Faraday rotation data taken in the Faraday geometry as a function of magnetic field and temperature. Data here were fit with a biexponential decay plus an offset: $A \exp(-t/T_1^a) + B \exp(-t/T_1^b) + C$, yielding spin lifetimes plotted in Figs. 8(c) and 8(d). As before, this should be viewed as a convenient parametrization of the data since the full decay of spin magnetization in these samples is more likely to be nonex-

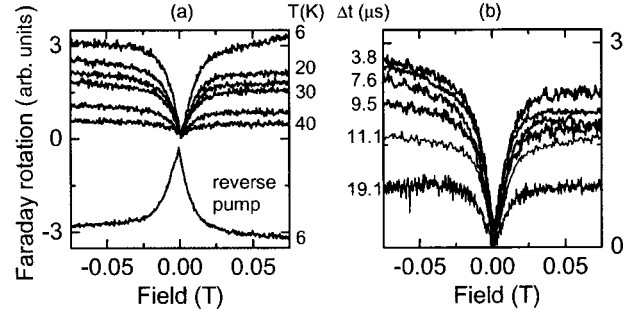


FIG. 9. (a) Changes in the microscale decay time of longitudinal spin polarization are inferred from the field and temperature dependence of the negative delay TRFR signal. $E_{\text{pump}} = 2.138$ eV, $E_{\text{probe}} = 2.102$ eV, $P_{\text{pump}} = 0.9$ mW, $P_{\text{probe}} = 100$ μ W. (b) Variation of the laser repetition interval provides a rough estimate of ~ 20 μ s for the decay time. $T = 5$ K. The pump power was varied to keep the energy per pulse constant: $P_{\text{pump}} = (2.1$ mW) (3.797 μ s/rep interval), $P_{\text{probe}} = 170$ μ W.

ponential. While the ~ 100 ps decay component decreases with field, the 10 ns-scale component dramatically increases over a surprisingly small range in the magnetic field of < 0.01 T before settling down to ~ 8 ns at $H = 1$ T. This dependence on the field is in distinct contrast to the proportionate reduction of transverse spin lifetimes by inhomogeneous dephasing. Although an increase in T_1 is consistent with simple expectations based on Boltzmann statistics, the field range over which this occurs corresponds to an energy scale (~ 6 μ eV) that is much smaller than $k_B T$ (400 μ eV at $T = 5$ K). The dependence on temperature also contrasts with the independence of transverse spin lifetimes up to ~ 150 K.⁶ Comparable lifetimes extracted from the TRA data in Fig. 5(f) suggest that carrier recombination may limit these longitudinal spin relaxation times.

Although often attributable to experimental artifacts, signals at negative time delay can correspond to an incomplete decay of spin polarization over the (~ 4 μ s) laser repetition interval.³⁸ Inspection of Figs. 8(a) and 8(b) indicates systematic changes in the negative delay signal with field and temperature, which reveal the presence of a microsecond scale decay component which accounts for the ‘‘offset’’ C in the biexponential function used above. This signal represents the weighted sum of contributions from preceding pump pulses in the pulse train, each separated by the laser repetition interval. Due to practical limitations of mechanical delay lines, we are unable to directly monitor the decay of Faraday rotation on this time scale although we can obtain information on changes in the decay time by monitoring the magnitude of the negative delay signal. Figure 9(a) shows Faraday rotation data taken at fixed time delay as a function of magnetic field. The signal arising from the microsecond-scale decay component decreases when the field is swept toward zero, forming a roughly symmetric ‘‘dip.’’ A field-induced increase in the long decay lifetime occurs over the ~ 20 mT width of the dip, which is comparable to that inferred from the data in Fig. 8(c) for the 10 ns-scale component. The sign of the dip reverses with pump helicity, verifying that the negative delay signal represents a preservation of longitudinal spin polarization over microseconds. The prominence of the dip is a mea-

sure of how fully the spin polarization decays within the repetition interval. The dip decreases with increasing temperature and is nearly absent by $T=40$ K, indicating the sensitivity of the long decay lifetime to thermal processes. As an indirect way to estimate the long-lifetime component, data were taken by electronically varying the repetition interval of the laser [Fig. 9(b)]. A plot of the signal at $H=-0.075$ T versus repetition interval roughly yields an estimate of ~ 20 μ s for the decay time. This number is significantly longer than previously measured photoluminescence lifetimes of ~ 1 μ s,^{15,31} perhaps suggesting that long spin polarization is exhibited in NC's where the electron and hole have been spatially separated. The suppression of radiative recombination through such separation may increase carrier lifetimes that otherwise could set an upper limit on measured spin lifetimes. Previous studies have suggested that charge separation through Auger-induced photoionization of NC's may be an important mechanism in determining the optical emission spectrum of individual NC's (Ref. 39) and energy relaxation.⁴⁰

The exact origin for the field and temperature dependencies of the long-time scale component is unclear. Here we speculate on one possible mechanism involving the hyperfine interaction with unpolarized nuclear spins.⁴¹ An important channel for electron spin relaxation in semiconductors is based on mutual spin flips between electrons and nuclei.⁴² Because many spin relaxation mechanisms in bulk semiconductors are absent in QD's, it has been suggested that spin flips with nuclei set an ultimate (although not necessarily realized) limit on the electron spin lifetime.⁵ Electron spin relaxation via hyperfine interactions results in a transfer of polarization to the nuclear spin system, so that nuclear polarization well in excess of equilibrium values can be maintained with optical illumination. Once a steady state nuclear polarization has been established, further electron spin relaxation via spin flips with nuclei is suppressed. This scenario then predicts that the changes in decay time inferred through temperature and field dependencies of the negative delay signal reflect changes in the efficiency by which the nuclear polarization can be maintained. The characteristic magnetic field width of the dips is similar in scale to dips measured in the hyperfine splitting of exciton states in GaAs QD's (~ 80 mT), which were attributed to nuclear depolarization that occurs when the applied field is smaller than fluctuations in the electron hyperfine field.⁴³ Dynamic nuclear polarization (DNP) via the hyperfine interaction is a temperature-dependent process whose efficiency starts to drop around 60 K,⁴⁴ which is not dissimilar to the temperature dependencies observed here. Although the temperature and field scales may be comparable to previous studies, we note that efforts to directly observe DNP in CdSe NC's using the techniques in Refs. 42 and 44 have been unsuccessful.

Because selection rules are poorly defined in the large majority of NC's whose c axis is oriented at a random angle, the boundaries between Faraday and Voigt geometries are blurred to the point that both electron and exciton spin precession have been observed in the Faraday geometry. Figure 10 shows data focusing on the early time dynamics where relatively weak oscillations are visible on top of the mono-

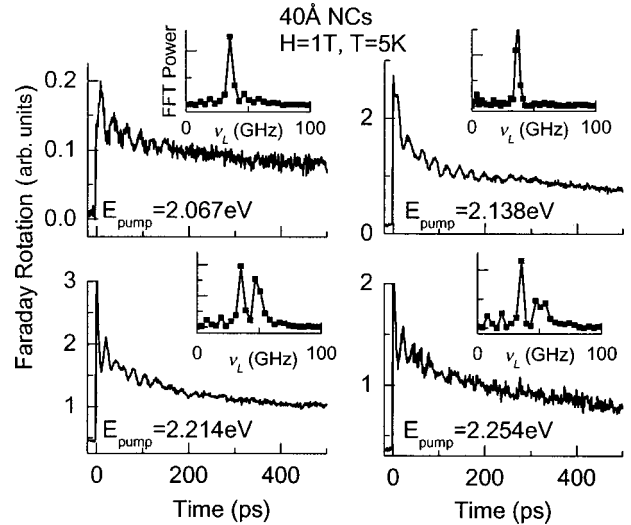


FIG. 10. Spin precession in the Faraday geometry with varying pump energy. FFT power spectra were calculated after subtracting the monotonically decaying background to reduce the baseline signal and improve peak visibility. Data were taken with $E_{\text{probe}} = 2.175$ eV, $P_{\text{pump}} = 2$ mW, $P_{\text{probe}} = 40$ μ W.

tonically decaying signal. The frequencies of precession are identical to data taken in the Voigt geometry, and oscillation lifetimes also decrease with magnetic field. Electron precession in the Faraday geometry might be attributable to the mixture of spin-up/spin-down conduction-band states that comprise the allowed exciton states¹⁴ or result from superpositions of exciton states generated in NC's whose c axis is at an angle to the field. Exciton precession seems to be sensitive to the choice of pump energy, with peak visibility occurring when E_{pump} is tuned in the vicinity of the $2S_{3/2}1S_e$ state. This dependence on E_{pump} is significantly different than in the Voigt geometry (Fig. 6), and might indicate that coherent superpositions of exciton spin states can be obtained upon relaxation from higher excited states. This will briefly be discussed in the Appendix.

VI. CONCLUSIONS

We have presented systematic studies of spin dynamics under both transverse and longitudinal magnetic fields. Interpretation of the experimental data is significantly complicated by the random orientation of nanocrystals that exhibit inherent anisotropy. We have developed an assignment of the multiple frequency components visible in spin precession to electron and exciton spins. While the assignment of one frequency component to electron precession is supported by the close agreement between experimental data and theoretical calculations, interpretation of the other frequency components in terms of exciton precession remains uncertain. The quasispherical model discussed in the Appendix can account for several aspects of the data, but also raises new questions concerning how coherent states are optically excited and preserved under energy relaxation. Inhomogeneous dephasing in these NC's follows the simple form expected for a Gaussian distribution of g factors, although the size distribution alone

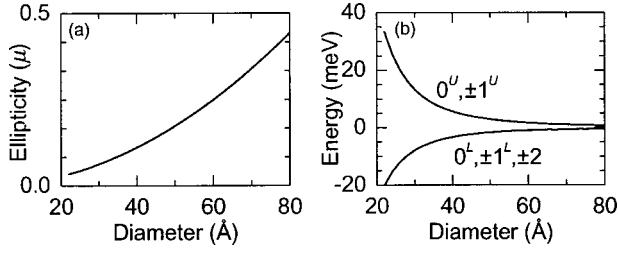


FIG. 11. (a) Calculation of ellipticity versus size needed to satisfy the quasispherical condition. (b) Calculation of fivefold and threefold degenerate exciton fine-structure levels for quasispherical NC's.

is insufficient to account for the observed dephasing rates. Additional contributions to the electron dephasing rate from anisotropy and surface conditions may also be important. Longitudinal spin lifetimes up to $\sim 20 \mu\text{s}$ are found to sensitively depend on applied field and temperature, exhibiting trends in both that are distinctly different than those measured for transverse spin lifetimes. The observation of spin precession in the Faraday geometry also raises questions about the nature of coherent states optically excited by circularly polarized light in these NC's.

ACKNOWLEDGMENTS

We are grateful to X. Peng, B. Boussert, and A. P. Alivisatos for NC synthesis and collaborative efforts and to M. Poggio for his assistance. This work was supported by grants from the DARPA (MDA972-01-1-0027), the NSF (DMR-0071888), and the ONR (N00014-99-1-0077).

APPENDIX: QUASISPHERICAL MODEL

The lifting of degeneracy for exciton states in CdSe NC's is due in part to the wurtzite crystal structure and nonspherical shape, both of which split states in the valence band according to the projection of hole angular momentum onto the c axis. As an example, the A, B excitons in bulk CdSe result from the splitting of heavy- and light-hole states by an energy $\Delta_{\text{cr}} \sim 25 \text{ meV}$. Similarly, it has been calculated that the nonspherical shape of CdSe NC's results in a splitting $\Delta_{\text{sh}} \propto -\mu/R^2$, where $(1 + \mu)$ is the NC aspect ratio and R is the NC radius.⁴⁵ The net splitting of the $1S_{3/2}$ hole states from the intrinsic crystal structure and the NC shape is the sum of the two terms: $\Delta_{\text{tot}} = \nu\Delta_{\text{cr}} + \Delta_{\text{sh}}$, and can equal zero for certain combinations of shape and size (ν is a numerical factor of order one for CdSe NC's).¹⁴ Figure 11(a) shows the ellipticity needed to satisfy the quasispherical condition for the range of NC sizes studied here. Given an expected variation in μ of $\sim \pm 0.2$, a significant fraction of NC's within the ensemble may satisfy this condition. The exciton g factors associated with the $1S_{3/2}1S_e$ states in quasi spherical NC's may be largely isotropic due to the lack of any preferred axis with respect to the applied magnetic field. The energies of exciton fine-structure states are solely determined by the electron-hole exchange interaction, which splits the initially eightfold degenerate exciton into two levels which are five-

fold and threefold degenerate according to $\mathbf{J}^{\text{tot}} = \mathbf{J}^h \pm \mathbf{S}$ (Ref. 14) [Fig. 11(b)].

The relation for g_{exc} in Eq. (3) can be calculated using expressions for the exciton wave functions from Ref. 14 evaluated in quasispherical NC's.

$$\Psi_1^L(r_e, r_h) = i \frac{\sqrt{3}}{2} \psi_{\uparrow, 1/2}(r_e, r_h) + \frac{1}{2} \psi_{\downarrow, 3/2}(r_e, r_h),$$

$$\Psi_{-1}^L(r_e, r_h) = \frac{i}{2} \psi_{\uparrow, -3/2}(r_e, r_h) + \frac{\sqrt{3}}{2} \psi_{\downarrow, -1/2}(r_e, r_h),$$

$$\Psi_1^U(r_e, r_h) = -\frac{i}{2} \psi_{\uparrow, 1/2}(r_e, r_h) + \frac{\sqrt{3}}{2} \psi_{\downarrow, 3/2}(r_e, r_h),$$

$$\Psi_{-1}^U(r_e, r_h) = \frac{1}{2} \psi_{\downarrow, -1/2}(r_e, r_h) - \frac{i\sqrt{3}}{2} \psi_{\uparrow, -3/2}(r_e, r_h),$$

$$\Psi_2(r_e, r_h) = \psi_{\uparrow, 3/2}(r_e, r_h), \quad \Psi_{-2}(r_e, r_h) = \psi_{\downarrow, -3/2}(r_e, r_h),$$

$$\Psi_0^{U,L}(r_e, r_h) = \frac{1}{\sqrt{2}} [\mp i \psi_{\uparrow, -1/2}(r_e, r_h) + \psi_{\downarrow, 1/2}(r_e, r_h)].$$

The ψ 's here represent $1S_{3/2}1S_e$ excitons with electron and hole angular momenta given by the subscripts. Expressed in the basis of state vectors ψ , the Hamiltonian matrix which describes the Zeeman splitting in an applied magnetic field can be derived from Eq. (30) in Ref. 14. In quasispherical NC's, one is free to assign the z axis to the magnetic-field direction, thus reducing Eq. (30) to the form

$$\hat{H}_{\text{Zeeman}} = \mu_B H_z \begin{bmatrix} \alpha & & & & & & & & \\ & \beta & & & & & & & \\ & & \gamma & & & & & & \\ & & & \delta & & & & & \\ & & & & -\delta & & & & \\ & & & & & -\gamma & & & \\ & & & & & & -\beta & & \\ & & & & & & & & -\alpha \end{bmatrix},$$

where

$$\alpha = (g_e - 3g_h)/2,$$

$$\beta = (g_e - g_h)/2,$$

$$\gamma = (g_e + g_h)/2,$$

$$\delta = (g_e + 3g_h)/2.$$

Effective exciton g factors in quasispherical NC's can then be calculated from relations like

$$g_{\text{exc}}^L \mu_B H_z = \langle \Psi_{+1}^L | \hat{H}_{\text{Zeeman}} | \Psi_{+1}^L \rangle - \langle \Psi_{-1}^L | \hat{H}_{\text{Zeeman}} | \Psi_{-1}^L \rangle.$$

Effective g factors for the different fine-structure states calculated using this procedure are

$$g_{\text{exc}}^{1L} = (g_e - 3g_h)/2,$$

$$g_{\text{exc}}^{1U} = -(g_e + 5g_h)/2,$$

$$g_{\text{exc}}^2 = (g_e - 3g_h).$$

The hole g factor g_h ($= -0.73$) was treated as a fitting parameter for the calculation of g_{exc} in Fig. 3 as there are no reliable experimental data for this quantity to our knowledge. While the calculated value of g_{exc}^{1L} agrees with the experimental data for the higher g -factor components in the entire sample set (using the same value of g_h), the other excitonic g factors in the 57 Å NC's cannot be accounted for with g_{exc}^{1U} or g_{exc}^2 .

Because the $\pm 1^L$ states in quasispherical NC's are optically inactive,¹⁴ it is expected that the initial excitation instead involves either the $\pm 1^U$ level or higher excited states (i.e., $2S_{3/2}1S_e$, etc.). These higher-lying states become increasingly inaccessible with decreasing E_{pump} , which may account for the decrease in exciton precession observed in Fig. 6. As mentioned previously, the time scale for relaxation among the fine-structure states is not well known. The sce-

nario presented here relies on the coherent relaxation of higher excited states to the $\pm 1^L$ level, which then exhibits a spin splitting corresponding to g_{exc}^{1L} . This is currently an open question that requires further study. Exciton precession in the Faraday geometry may be explained with similar arguments. *A priori*, exciton precession in this geometry is unexpected, since well-defined optical selection rules for the $1S_{3/2}1S_e$ state in quasispherical NC's dictate that circularly polarized light directly excites a particular spin eigenstate rather than superpositions of eigenstates. Such restrictions do not hold for excitation into higher excited states; the exciton might then relax coherently into the ground state and precess as usual.

Definitive understanding of exciton precession in these NC's is difficult given the uncertain nature of the energy spectrum and optical selection rules over the ensemble of NC's. While the quasispherical model addresses this difficulty, it raises a host of additional questions related to the nature of coherent excitation. Analogous studies of spin dynamics in related materials, such as CdTe NC's (which have a cubic crystal structure), may yield further insight into these problems.

*Author to whom correspondence should be addressed. Email address: awsch@physics.ucsb.edu

†On leave from A. F. Ioffe Physico-Technical Institute.

¹M. Grundmann, *Physica E (Amsterdam)* **5**, 167 (2000).

²M. Bruchez, Jr., M. Moronne, P. Gin, S. Weiss, and A. P. Alivisatos, *Science* **281**, 2013 (1998).

³S. A. Wolf, D. D. Awschalom, R. A. Buhrman, J. M. Daughton, S. von Molnar, M. L. Roukes, A. Y. Chtchelkanova, and D. M. Treger, *Science* **294**, 1488 (2001).

⁴D. Loss and D. P. DiVincenzo, *Phys. Rev. A* **57**, 120 (1998).

⁵I. A. Merkulov, Al. L. Efros, and M. Rosen, *Phys. Rev. B* **65**, 205309 (2002).

⁶J. A. Gupta, D. D. Awschalom, X. Peng, and A. P. Alivisatos, *Phys. Rev. B* **59**, 10 421 (1999).

⁷A. V. Rodina, Al. L. Efros, M. Rosen, and B. K. Meyer, *Mater. Sci. Eng., C* **19**, 435 (2002); A. V. Rodina, Al. L. Efros, A. Yu. Alekseev and B. K. Meyer (unpublished).

⁸C. B. Murray, D. J. Norris, and M. G. Bawendi, *J. Am. Chem. Soc.* **115**, 8706 (1993); J. E. Bowen-Katari, V. L. Colvin, and A. P. Alivisatos, *J. Phys. Chem.* **98**, 4109 (1994).

⁹A. V. Kadavanich, Ph.D. dissertation, University of California, Berkeley, 1997.

¹⁰X. Peng, M. C. Schlamp, A. V. Kadavanich, and A. P. Alivisatos, *J. Am. Chem. Soc.* **119**, 7019 (1997).

¹¹A. I. Ekimov, F. Hache, M. C. Schanne-Klein, D. Ricard, C. Flytzanis, I. A. Kudryavtsev, T. V. Yazeva, A. V. Rodina, and Al. L. Efros, *J. Opt. Soc. Am. B* **10**, 100 (1993).

¹²D. J. Norris and M. G. Bawendi, *Phys. Rev. B* **53**, 16 338 (1996).

¹³D. J. Norris, Al. L. Efros, and M. G. Bawendi, *Phys. Rev. B* **53**, 16 347 (1996).

¹⁴Al. L. Efros, M. Rosen, M. Kuno, M. Nirmal, D. J. Norris, and M. G. Bawendi, *Phys. Rev. B* **54**, 4843 (1996).

¹⁵M. Nirmal, D. J. Norris, M. Kuno, M. G. Bawendi, Al. L. Efros, and M. Rosen, *Phys. Rev. Lett.* **75**, 3728 (1995).

¹⁶M. Nirmal and M. G. Bawendi (unpublished).

¹⁷J. A. Gupta and D. D. Awschalom, *Phys. Rev. B* **63**, 085303 (2001).

¹⁸S. A. Crooker, D. D. Awschalom, J. J. Baumberg, F. Flack, and N. Samarth, *Phys. Rev. B* **56**, 7574 (1997).

¹⁹B. E. A. Saleh and M. C. Teich, *Fundamentals of Photonics* (Wiley, New York, 1991).

²⁰Plotted for clarity is the FFT power spectrum, typically computed from a subset of the data that excludes the sharp peak at $t=0$. When significant, nonoscillatory backgrounds were subtracted from the data prior to calculation of the FFT.

²¹W. W. Piper, in *Proceedings of the 7th International Conference on II-VI Semiconductor Compounds*, edited by D. G. Thomas (Benjamin, New York, 1967), p. 839.

²²L. M. Roth, B. Lax, and S. Zwerdling, *Phys. Rev.* **114**, 90 (1959).

²³A. A. Kiselev, E. L. Ivchenko, and U. Rössler, *Phys. Rev. B* **58**, 16 353 (1998).

²⁴A. V. Kapustina, B. V. Petrov, A. V. Rodina, and R. P. Seisyan, *Fiz. Tverd. Tela* **42**, 207 (2002) [*Phys. Solid State* **42**, 1242 (2000)].

²⁵D. G. Thomas and J. J. Hopfield, *Phys. Rev.* **175**, 1021 (1968).

²⁶M. Kuno, M. Nirmal, M. G. Bawendi, Al. L. Efros, and M. Rosen, *J. Chem. Phys.* **108**, 4242 (1998).

²⁷J. A. Gupta, Ph.D. dissertation, University of California, Santa Barbara, 2002.

²⁸Al. L. Efros (unpublished).

²⁹T. Amand, X. Marie, P. Le Jeune, M. Brousseau, D. Robart, J. Barrau, and R. Planel, *Phys. Rev. Lett.* **78**, 1355 (1997).

³⁰U. Woggon, H. Giessen, F. Gindele, O. Wind, B. Fluegel, and N. Peyghambarian, *Phys. Rev. B* **54**, 17 681 (1996).

³¹E. Johnston-Halperin, D. D. Awschalom, S. A. Crooker, Al. L. Efros, M. Rosen, X. Peng, and A. P. Alivisatos, *Phys. Rev. B* **63**, 205309 (2001).

³²P. Palinginis and H. Wang, *Appl. Phys. Lett.* **78**, 1541 (2001).

- ³³V. I. Klimov and D. W. McBranch, Phys. Rev. Lett. **80**, 4028 (1998).
- ³⁴Two calibration factors were necessary to ensure that quantitative analysis of FFT linewidths produced correct values of Δ_f . The first relates the linewidths of the FFT magnitude and power spectra. While we could more reliably fit the power spectra, it is the linewidth of the FFT magnitude that is directly related to Δ_t . The second factor accounts for the fact that true Gaussian transforms are obtained only if the time-domain data are symmetric about $t=0$. These factors were derived from analysis of simulated TRFR data using Eq. (6); the consistency of the procedure was checked with various values of Δ_g and H .
- ³⁵The sole exception to this rule is the 40 Å core/shell NC sample, where the electron and exciton dephasing rates are nearly equal.
- ³⁶X. Peng (personal communication).
- ³⁷C. Hermann and C. Weisbuch, Phys. Rev. B **15**, 823 (1977).
- ³⁸J. M. Kikkawa and D. D. Awschalom, Phys. Rev. Lett. **80**, 4313 (1998).
- ³⁹S. A. Empedocles, D. J. Norris, and M. G. Bawendi, Phys. Rev. Lett. **77**, 3873 (1996).
- ⁴⁰V. I. Klimov and D. W. McBranch, Phys. Rev. B **55**, 13 173 (1997).
- ⁴¹Additional motivation for this speculation arises from data taken in CdS NC's prepared in a glass matrix (Ref. 27). Both CdSe and CdS NC's showed microsecond scale nonprecessing spin polarization in the Faraday and Voigt geometries. Observation of nonprecessing magnetization in the Voigt geometry is probably due to the random orientation of NC's in the sample. In CdS NC's, careful examination of the negative delay signal in the Voigt geometry at low fields (<3 mT) revealed W features similar to Hanlé effect data previously attributed to electron-nuclear hyperfine interactions in III-V bulk semiconductors (Ref. 42). Similar albeit less thorough measurements of the negative delay signal in CdSe NC's showed no such features, for reasons which are unclear at present.
- ⁴²*Optical Orientation*, edited by F. Meier and B. P. Zakharchenya (Elsevier, Amsterdam, 1984).
- ⁴³D. Gammon, Al. L. Efros, T. A. Kennedy, M. Rosen, D. S. Katzer, D. Park, S. W. Brown, V. L. Korenev, and I. A. Merkulov, Phys. Rev. Lett. **86**, 5176 (2001).
- ⁴⁴G. Salis, D. T. Fuchs, J. M. Kikkawa, D. D. Awschalom, Y. Ohno, and H. Ohno, Phys. Rev. Lett. **86**, 2677 (2001).
- ⁴⁵Al. L. Efros and A. V. Rodina, Phys. Rev. B **47**, 10 005 (1993).